

Shear testing of stacked bonded masonry

Juliana T. Oliveira, Paulo B. Lourenço, Joaquim O. Barros

Report 02-DEC/E-10

*The present research has been carried out under
contract GROW-1999-70420 “ISO-BRICK” from the European Commission*

DRAFT VERSION

Date: October 2002

No. of pages: 33

Keywords: Shear Testing, Triplet Test, Joints Infilled with Concrete.



Escola de
Engenharia



Departamento de
Engenharia Civil



Universidade
do Minho



Contents

1 Introduction	3
2 Characterization of the Materials.....	4
2.1 Clay Units	4
2.1.1 Half unit tests under compressive load applied along X direction.....	5
2.1.2 Full unit tests under compressive load applied along X direction	7
2.1.3 Half unit tests under compressive load applied along Y direction.....	8
2.2 Concrete Joints.....	10
3 Results of the Shear Tests.....	12
3.1 Description of the testing procedure.....	12
3.2 Description of the test set-up	12
3.3 Test Results.....	15
3.3.1 Series 1 – Panels B1, B2 and B3.....	15
3.3.2 Series 2 – Panels B4, B5 and B6.....	18
3.3.3 Series 3 – Panels B7, B8 and B9.....	20
3.3.4 Definition of the Joint Strength Parameters	22
3.3.5 Evaluation of the dilatancy.....	24
4 Conclusions	26
5 References	27
ANNEX A.....	28



1 Introduction

This report presents the results of a series of shear tests in masonry panels carried out according to EN 1052-4 – “Methods of test for masonry – Part 4: Determination of shear strength including damp proof course” (CEN, 2000). Given the stacked nature of the masonry panels and the novel use of micro-concrete it is essential to use this standard instead of the triplet test detailed in prEN 1052-3 – “Methods of test for masonry – Part 3: Determination of initial shear strength” (CEN, 1996).

In total, nine masonry specimens have been tested, in three series associated with three different normal pre-compression levels.

Additionally, the strength values of the masonry units and micro-concrete used for the joints have been also characterized.

2 Characterization of the Materials

2.1 Clay Units

The clay units used in the masonry panels have been produced by J. Monteiro & Filhos, Lda, in Portugal, especially for the current research project. The units have been produced and delivered in a single batch. The unit dimensions are 215mm (length), 100mm (width) and 65mm (height), see Figure 2-1. The unit is hollow with two holes of 25mm × 25mm.

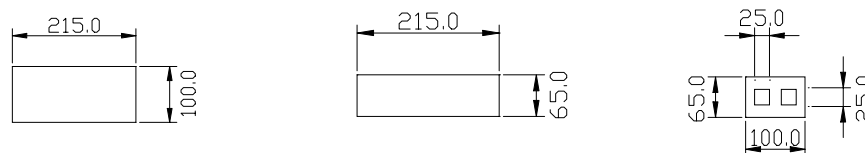


Figure 2-1 – Geometry of clay units.

Due to the anisotropy associated with the extrusion process and firing, the uniaxial compression tests were carried out in two orthogonal directions, namely along the length (X direction) and height (Y direction) of the unit, as illustrated in Figure 2-2.

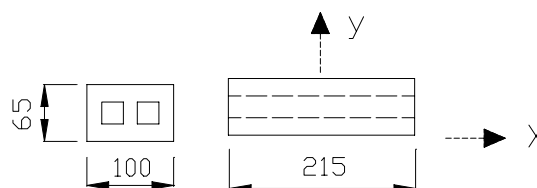


Figure 2-2 – Directions for testing the units under compression loading.

The tests were carried out according to EN 772-1 – “Methods of test for masonry units: Determination of compression strength”, (CEN, 2000). For the X direction, two different specimens were used, consisting of half units and full units. For the Y direction, only half unit specimens were used. The surface of all specimens was treated with grinding equipment so that planarity of the loading faces could be ensured. It is noted that the clay units exhibited different colors, typical of units with different firing temperatures.

All tests were carried out in dry specimens. The ground specimens were stored at constant temperature of $105^{\circ}\text{C} \pm 5^{\circ}\text{C}$ in stove, until constant mass was reached. A universal testing machine with a maximum loading capacity of 3000 kN was used for the tests.

2.1.1 Half unit tests under compressive load applied along X direction

For this purpose, the units were mechanically sawn in half. Eight specimens were tested, denoted by CXH. Figure 2-3 illustrates the sides of the unit and their designations. The load was applied with a velocity of 120 kN/minute.

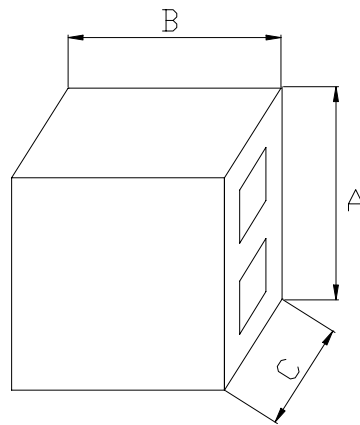


Figure 2-3 – Sides of the unit.

Table 2-1 gives the dimensions of each surface, the collapse load, the net compressive strength $f_{b, \text{net}}$ and the apparent compressive strength $f_{b, \text{app}}$, for the X direction. The dimension of the holes was assumed equal to 25×25 in mm^2 . In addition, also the average strength values and the coefficient of variation (C.V.) is indicated. The coefficient of variation encountered is around 26%, which is rather large for the uniaxial compressive strength. It is likely that the different firing temperature of this special purpose unit justifies the scatter encountered. At a later stage of production stage, this scatter is expected to be lowered up to 10%.

Table 2-1– Dimensions and strength of the units, for X compression and half units.

Specimen	Color	A (mm)	B (mm)	C (mm)	Maximum Load (kN)	$f_{b, net}$ (MPa)	$f_{b, app}$ (MPa)
CXH.1	Light	103	103	65	576.1	105.80	86.05
CXH.2	Dark	105	105	65	560.6	100.56	82.14
CXH.3	Light	105	105	65	295.0	52.91	43.22
CXH.4	Light	103	105	65	511.5	93.94	76.40
CXH.5	Dark	100	105	65	567.0	108.00	87.23
CXH.6	Light	103	103	65	452.6	83.12	67.60
CXH.7	Dark	100	100	65	649.0	123.62	99.85
CXH.8	Dark	100	100	65	736.0	140.19	113.23
Average						101.02	81.97
C.V. (%)						25.93	

The net area of side AC, for the calculation of the net compressive strength, is obtained from $(C \times A) - 2 \times (25 \times 25)$ in mm^2 , being given in Table 2-2. Failure of the units was rather brittle and explosive, as illustrated in Figure 2-4.

Table 2-2 – Net area of side AC, for X compression and half units.

CXH.1	5445
CXH.2	5575
CXH.3	5575
CXH.4	5445
CXH.5	5250
CXH.6	5445
CXH.7	5250
CXH.8	5250



Figure 2-4 – Typical failure of the specimens tested along the X direction, half unit.

2.1.2 Full unit tests under compressive load applied along X direction

Again, eight specimens were tested, denoted now by CXF. Table 2-3 gives the dimensions of each surface, the collapse load, the net compressive strength $f_{b, net}$ and the apparent compressive strength $f_{b, app}$, for the X direction. A column indicates the color of the unit as the compressive strength is clearly correlated with this feature. In addition, also the average strength values and the coefficient of variation (C.V.) are indicated.

The coefficient of variation is even larger for this series (35%) but two groups of results are clearly noticeable, associated with the color of the units. In these two groups, the strength variation is acceptable. The apparent strength of the present series (71.83 MPa) is 12% lower than the apparent strength of the series using half units (81.97 MPa). It is likely that this strength reduction is associated with the lower confinement of the steel platens for the full unit tests. The results using the full units should be used for all purposes.

Table 2-3 – Dimensions and strength of the units, for X compression and full units.

Specimen	Color	A (mm)	B (mm)	C (mm)	Maximum Load (kN)	$f_{b, net}$ (MPa)	$f_{b, app}$ (MPa)
CXF.1	Light	105	105	65	290.07	52.03	42.50
CXF.2	Light	105	105	65	321.85	57.73	47.16
CXF.3	Light	105	105	65	349.67	62.72	51.23
CXF.4	Light	105	105	65	369.54	66.29	54.15
CXF.5	Dark	100	100	65	611.92	116.56	94.14
CXF.6	Dark	100	100	65	611.92	116.56	94.14
CXF.7	Dark	100	100	65	596.03	113.53	91.70
CXF.8	Dark	100	100	65	647.68	123.37	99.64
Average						88.60	71.83
C.V.						35.31	

The net area of side AC, for the calculation of the net compressive strength, is again obtained from $(C \times A) - 2 \times (25 \times 25)$ in mm^2 , being given in Table 2-4. A typical failure mode is illustrated in Figure 2-5.

Table 2-4 – Net area of side AC, for X compression and full units.

CXF.1	5575
CXF.2	5575
CXF.3	5575
CXF.4	5575
CXF.5	5250
CXF.6	5250
CXF.7	5250
CXF.8	5250

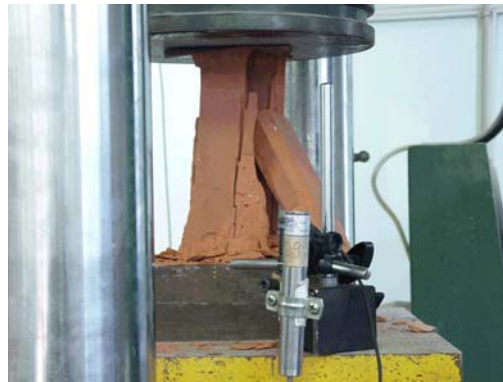


Figure 2-5 – Typical failure of the specimens tested along the X direction, full unit.

2.1.3 Half unit tests under compressive load applied along Y direction

Again, eight specimens were tested, denoted now by CYF. Along Y direction, the load was applied with a velocity of 75 kN/minute. Table 2-5 gives the dimensions of each surface, the collapse load, the net compressive strength $f_{b, net}$ and the apparent compressive strength $f_{b, app}$, for the Y direction. In addition, also the average strength values, the coefficient of variation (C.V.) and a column indicating the color are given. The coefficient of variation encountered is around 12%, which is smaller than the values observed for the tests carried out along the X direction. The net compressive strength along the Y direction (53.29 MPa) is only 60% of the net compressive strength along the X direction (88.60 MPa), which is probably due to the fact that extrusion of the unit occurs along the X direction. It is stressed that, due to the horizontal holes, the apparent compressive strength along the Y direction (32.79 MPa) is only 45% of the apparent compressive strength along the X direction (71.83 MPa), which indicates a highly anisotropic material.

Table 2-5 – Dimensions and strength of the units, for Y compression and half units.

Specimen	Color	A (mm)	B (mm)	C (mm)	Maximum Load (kN)	$f_{b, net}$ (MPa)	$f_{b, app}$ (MPa)
CYH.1	Dark	97.0	110.0	65.0	251.5	57.16	35.17
CYH.2	Dark	95.0	105.0	65.0	244.4	58.19	35.81
CYH.3	Light	102.0	110.0	65.0	139.3	31.66	19.48
CYH.4	Dark	97.0	110.0	65.0	304.3	69.16	42.56
CYH.5	Light	100.0	105.0	65.0	158.6	37.76	23.24
CYH.6	Light	100.0	105.0	65.0	201.6	48.00	29.54
CYH.7	Light	97.0	105.0	65.0	216.3	51.50	31.69
CYH.8	Dark	95.0	108.0	65.0	314.9	72.89	44.86
Average						53.29	32.79
C.V.						11.49	

The net area considered on Y direction was calculated from $(C - 25) \times B$ in mm^2 . The net area, for the calculation of the net compressive strength, is presented in Table 2-6. Failure of the units was rather brittle and explosive, as illustrated in Figure 2-6.

Table 2-6 – Net area, for Y compression and half units.

CYH.1	4400
CYH.2	4200
CYH.3	4400
CYH.4	4400
CYH.5	4200
CYH.6	4200
CYH.7	4200
CYH.8	4320



Figure 2-6 – Typical failure of the specimens tested along the Y direction, half unit.

2.2 Concrete Joints

The masonry joints have a thickness of only 25 mm and will be filled with a micro-concrete, made using small aggregate size. The final masonry roof shells envisaged in the current project are to be reinforced with steel rebars in the joints. Thus, a special purpose concrete mix with a high slump is required. The adopted mix has been proposed by Prégua, SA, for prefabrication and consists of 360Kg of cement, 615Kg of gravel, 1208Kg of sand, 174L of water and 3.60L of Superplastifier Rebuilt 1000, per m³, which returns a slump of 16 cm. This mix has been designed in order to obtain a class C30/35 concrete.

Figure 2-7 illustrates the compression and tension tests carried out to characterize the mechanical behavior of the concrete. The compressive strength f_c was obtained using the average of four cylindrical specimens, according to the recommendations of RILEM CPC4 (1994). The tensile strength $f_{t,fl}$ was obtained using the average of four notched concrete beams, according to the recommendations of RILEM FMC1 (1994). The results of these tests, at 28 days, are given in Table 2-7.

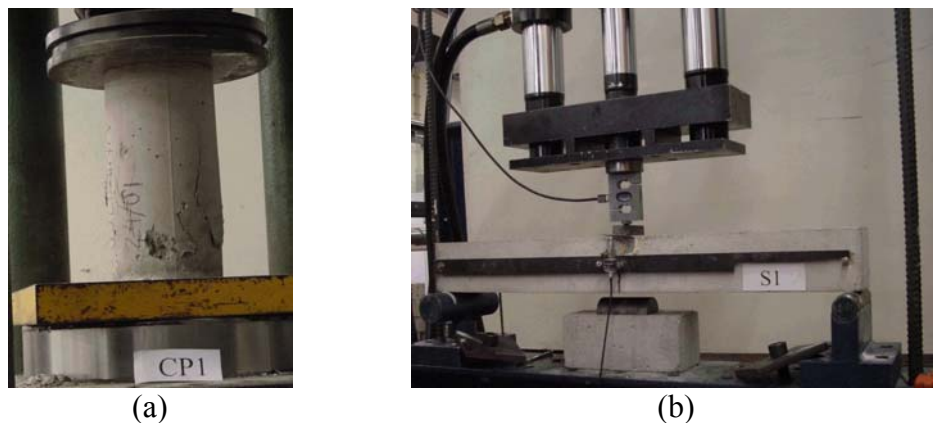


Figure 2-7 – Tests carried out to characterize the adopted concrete mix: (a) uniaxial compression test on cylindrical specimens of concrete and (b) three-point bending tests on prismatic beams.



Table 2-7 – Results of the concrete tests.

Specimen	f_c (MPa)	$f_{t, fl}$ (MPa)
1	29.93	1.76
2	28.60	1.70
3	31.53	1.75
4	30.95	1.68
Average	30.25	1.73

3 Results of the Shear Tests

3.1 Description of the testing procedure

According to EN 1052-4, the specimens consist of three masonry courses subjected to a vertical precompression load, see Figure 3-1. The top and bottom masonry courses are kept under constant pressure while a horizontal load is applied in the middle masonry course. Eventually this course slides, providing the value of the shear strength of the joints. Therefore, two joints are tested simultaneously.

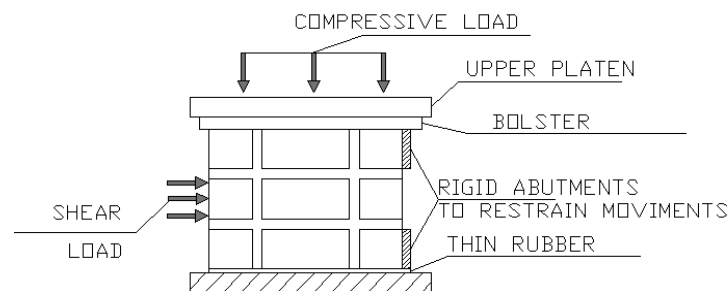


Figure 3-1 – Testing procedure according to EN 1052-4.

In order to define the cohesion and the friction angle of the joints, three different pre-compression stress levels were adopted, namely 0.2N/mm^2 , 0.6N/mm^2 and 1.0N/mm^2 . These stress levels were kept constant during the complete tests duration. For each pre-compression stress level, three panels were tested as required by the norm, resulting in a total of nine tests.

The specimens were divided in three series: Series 1 for a pre-compression level of 0.2N/mm^2 (panels B1 to B3), Series 2 for a pre-compression level of 0.6N/mm^2 (panels B4 to B6) and Series 3 for a pre-compression level of 1.0N/mm^2 (panels B7 to B9).

3.2 Description of the test set-up

Figure 3-2 shows the test set-up. Two horizontal rubber supports restricted the movement of the top and bottom courses of the panel. These supports are pinned and cover

the full height of the course in order to minimize any bending effect of the panel, see Figure 3-3a. The horizontal and vertical loading system consisted of two independent actuators, as shown in Figure 3-3b,c. The horizontal actuator was applied directly on the middle course and the vertical actuator was applied on a steel beam, so that the load could be distributed in the panel.

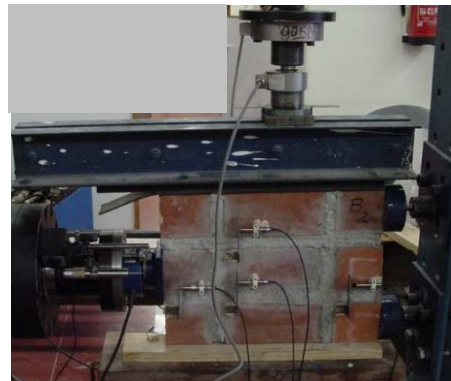


Figure 3-2 – General view of the test set-up.

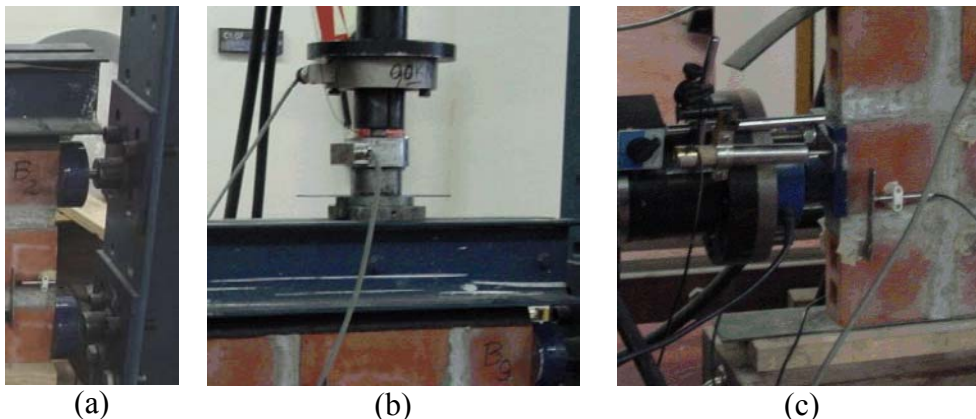


Figure 3-3 – Details of the test set-up: (a) supports adopted to restrict the horizontal movement of the top and bottom courses; (b) vertical actuator and load cell; (c) horizontal actuator with load cell and LVDT for displacement control.

Initially, the vertical compressive load was applied by means of the vertical hydraulic actuator under force control at a rate of 10kN per minute. The maximum loading capacity of the vertical actuator is 50kN. Subsequently, this hydraulic actuator was kept under force control resulting in a vertical load almost constant. Figure 3-4 illustrates the time history of the vertical load for each panel series. It can be observed that the vertical

load was kept approximately constant during the test duration, with the exception of some sudden load peaks due to the irregularity in the failure surfaces of the joints. As a consequence the top steel beam was allowed to move in the vertical direction.

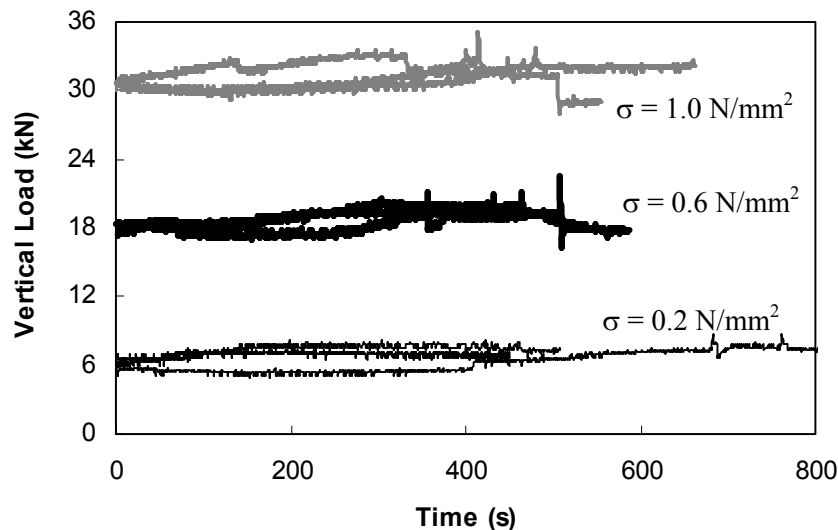


Figure 3-4 – Chronological history of the vertical load applied to panels under force control (σ is the pre-compression level).

After the application of the selected pre-compression level, the horizontal load was applied by imposing small displacement increments with a hydraulic actuator of a maximum loading capacity equal to 250kN. The horizontal shear load, measured with a load cell, was applied with a velocity of 15kN per minute.

The displacements of the panel were recorded with eight linear voltage displacement transducers (LVDTs). Four LVDTs were placed on the front of the specimens to measure the displacements in the shear direction and three LVDTs were placed on the back of the specimen to measure the vertical displacements. As stated above, one LVDT was located at the horizontal actuator so that the test could be carried out under displacement control. The positions of the LVDTs are illustrated in Figure 3-5 and Figure 3-6.

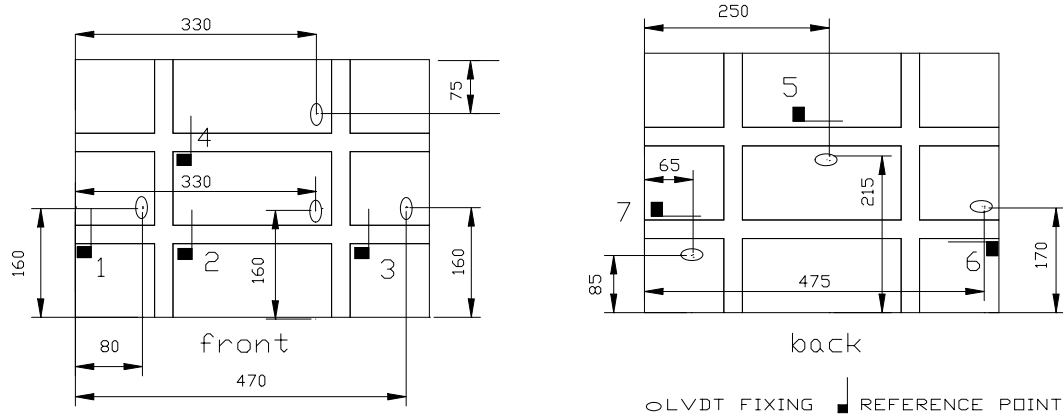


Figure 3-5 – Location of LVDTs in the panels, with dimensions in mm.

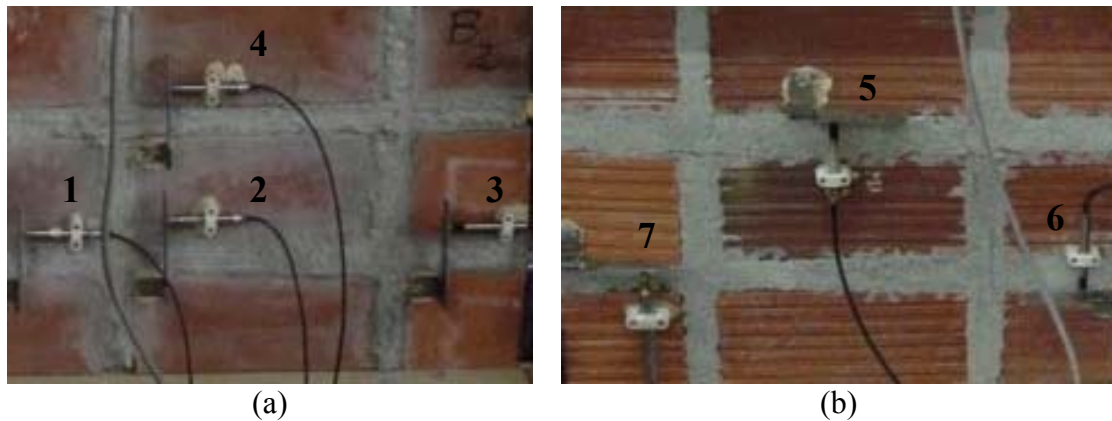


Figure 3-6 – Panel ready for testing with LVDTs installed : (a) front view, with horizontal LVDTs no. 1 – 4 and (b) back view, with vertical LVDTs no. 5 – 7.

3.3 Test Results

3.3.1 Series 1 – Panels B1, B2 and B3

Figure 3-7 shows the relation between the shear load and the horizontal displacement at the joints for series 1. Here, the horizontal displacement represents a weighted average of the measurements recorded using LVDTs 1-4, placed on the horizontal direction. Figure 3-8 illustrates the relation between the horizontal displacements of the two horizontal joints. Here, the bottom joint value is the average of the recordings from LVDTs 1-3 and the top joint value is the recording of LVDT 4.

Finally, Figure 3-9 presents the failure mode of the panels. It is noted that the variation of the recordings from LVDTs 1-3 is usually minimal. The sole exception is the case of complex failure modes that include head joints or diagonal cracks through the units.

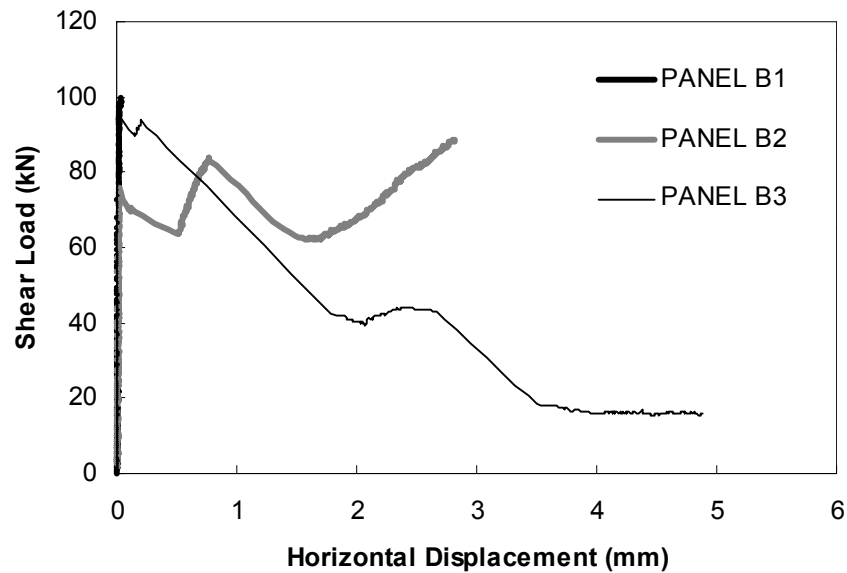


Figure 3-7 – Shear load vs. horizontal displacement - series 1.

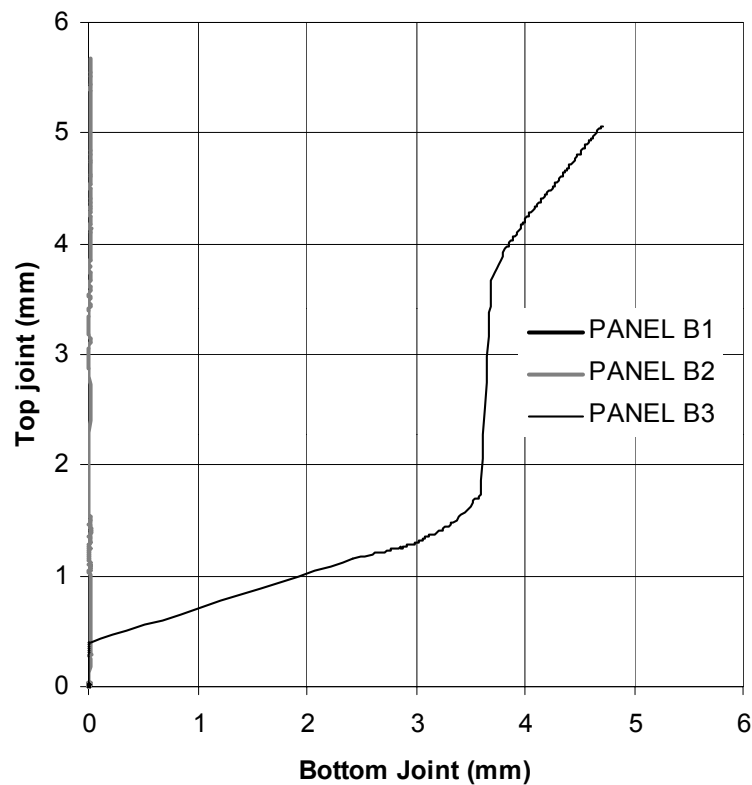


Figure 3-8 – Relation between the horizontal displacements of the joints - series 1.

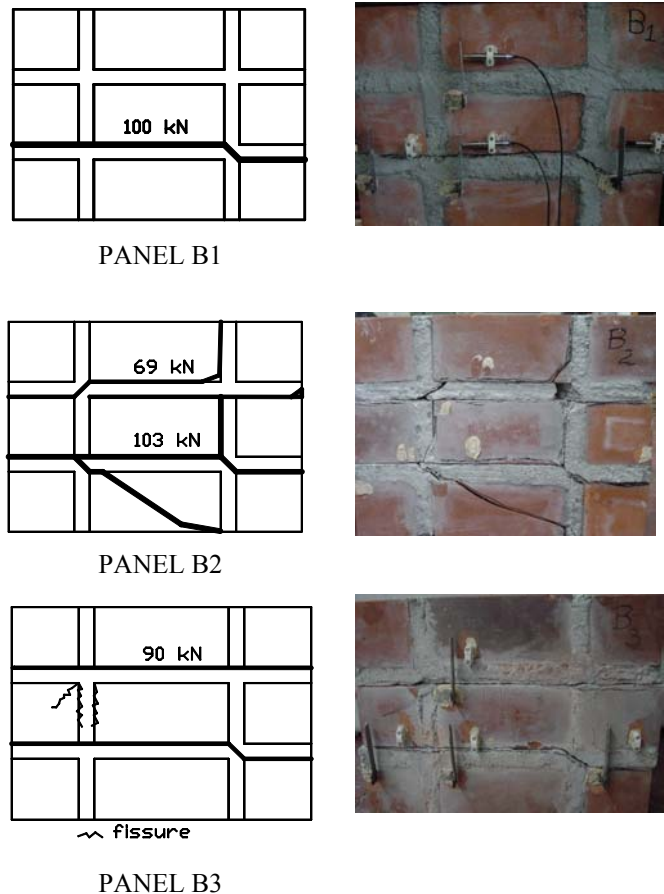


Figure 3-9 – Failure mode of the panels - series 1.

The post-peak response of panel B1 could not be recorded but the post-peak response of panels B2 and B3 could be recorded until termination of the test.

Panel 1 collapse exhibits a stepped crack at the bottom joint and minor diffused cracked at the top joint. This indicates a probable displacement at the right top support that lead to minor sliding of the top joint. The collapse load of this test was similar to the other two tests, which indicates that both joints effectively slide.

In panel 2, the cracks deviated from the horizontal joints and progressed through the units and head joints. This can be due to the presence of firing cracks in the joints and deficiently executed head joints. The existence of gravel in the crossed joint can also preclude the crack propagation along the interface. This peculiar shape of collapse is stressed in Figure 3-8, where it is clear that a significant average relative displacement of the LVDTs in the bottom joint could not be recorded. This also indicates that the use of an average horizontal displacement in Figure 3-7 is debatable, for this particular panel.

The results for Panel B3 in term of force-displacement diagram are coherent and follow the expected pattern. The residual plateau found in the response is associated with the friction of the joint. Nevertheless, a sudden increase of strength is observed for an average displacement of 2.0mm. This corresponds to the sudden jump in the diagram of Figure 3-8. It is believed that the different displacements in the top and bottom joint are related to interlocking associated with the gravel size and to movements in the lateral supports. This clearly demonstrates the complexity of the phenomena involved in the failure of the triplet test, see also Jukes and Riddington (2001).

Finally, the failure modes illustrated in Figure 3-9 show a clear trend for the occurrence of stepped crack in the right side of the joints, in the intersection of horizontal and vertical joints. It is believed that this stepped crack is due to the presence of the horizontal right supports in the top and bottom masonry courses, which induce a significant rotation of the normal stresses in the mortar joint.

3.3.2 Series 2 – Panels B4, B5 and B6

Figure 3-10 shows the relation between the shear load and the horizontal displacement at the joints for series 2. Due to the higher pre-compression level, the maximum shear load was increased. Figure 3-11 illustrates the relation between the horizontal displacements of the two horizontal joints. Finally, Figure 3-12 presents the failure mode of the panels.

The results for Panel B4 in term of force-displacement diagram are coherent and follow the expected pattern. This panel failed simultaneously in the top and bottom joints as indicated in Figure 3-12. This can be understood from Figure 3-11, where a continuous relation between the displacements in the top and bottom joints is found.

The joints in Panels B5 and B6 have failed in a similar way. Initially, only one joint has failed but, upon reloading, a second crack developed at the non-cracked interface. This is clearly in agreement with the diagrams in Figure 3-11, where it can be seen that sliding in the bottom joint is not accompanied with sliding in the top joint, until a significant relative displacement is found. In Panel B6, it can be observed that global softening only occurs once both top and bottom cracks are formed, at an average horizontal displacement equal to circa 1.3mm (or a displacement in the bottom joint of circa 2.6mm).

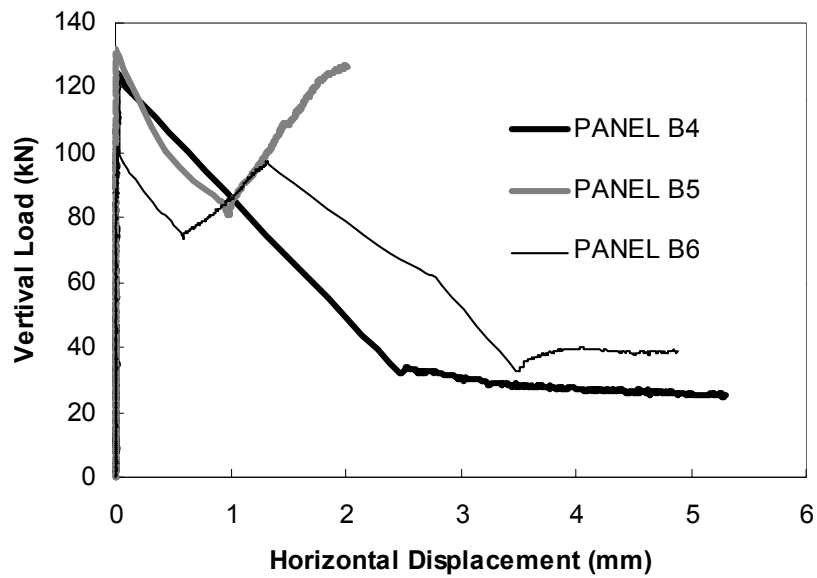


Figure 3-10 – Shear load vs. horizontal displacement - series 2.

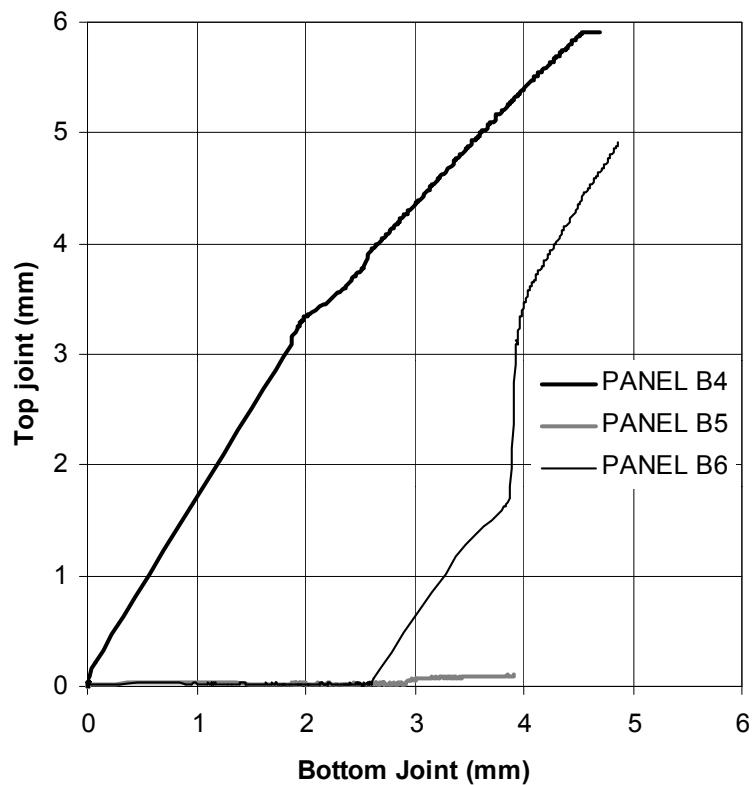


Figure 3-11 – Relation between the horizontal displacements of the joints - series 2.

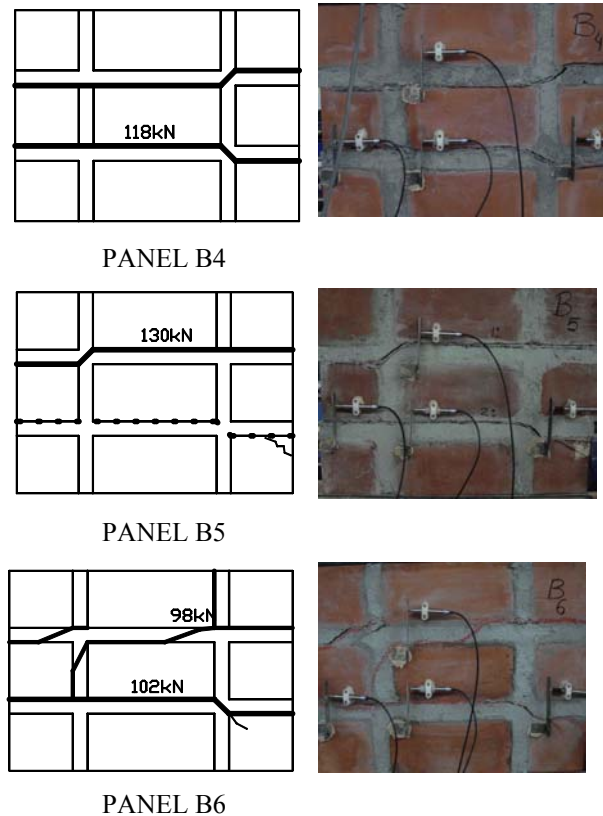


Figure 3-12 – Failure mode of the panels - series 2.

3.3.3 Series 3 – Panels B7, B8 and B9

Figure 3-13 shows the relation between the shear load and the horizontal displacement at the joints for series 3. Due to the higher pre-compression level, again the maximum shear load was increased. Figure 3-14 illustrates the relation between the horizontal displacements of the two horizontal joints. Finally, Figure 3-15 presents the failure mode of the panels.

The post-peak response of panel B7 could not be recorded but the post-peak response of panels B8 and B9 could be recorded until termination of the test.

Panel B7 exhibited a full crack of the bottom joint at a load of 120kN. This crack resulted in a rigid body rotation between the top and bottom part.

Panel B8 and Panel B9 exhibited different load-displacement diagrams. The response of Panel B9 follows the expected pattern whereas a very ductile response was found for Panel B8. The first crack occurred in the top joint, as it can be seen in Figure 3-14.

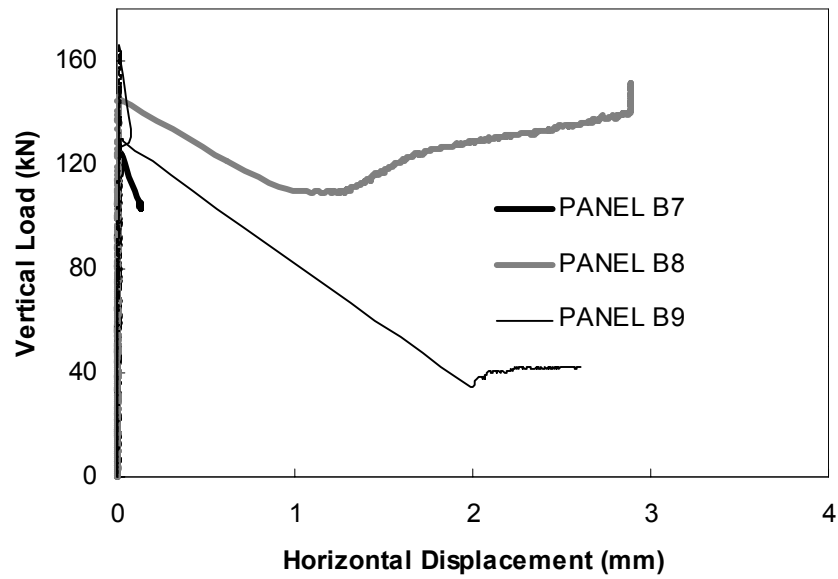


Figure 3-13 – Shear load vs. horizontal displacement - series 3.

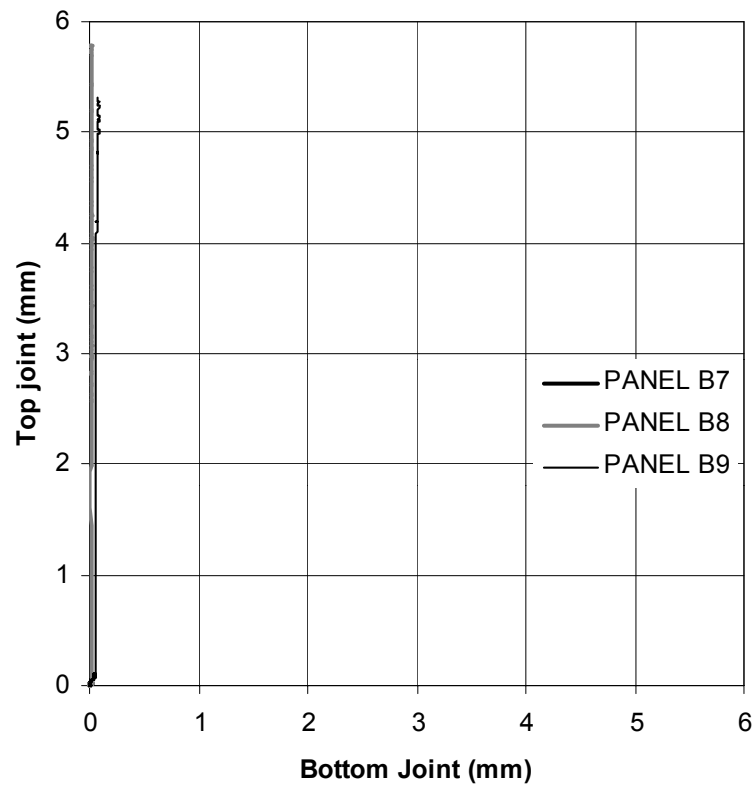


Figure 3-14 – Relation between the horizontal displacements of the joints - series 3.

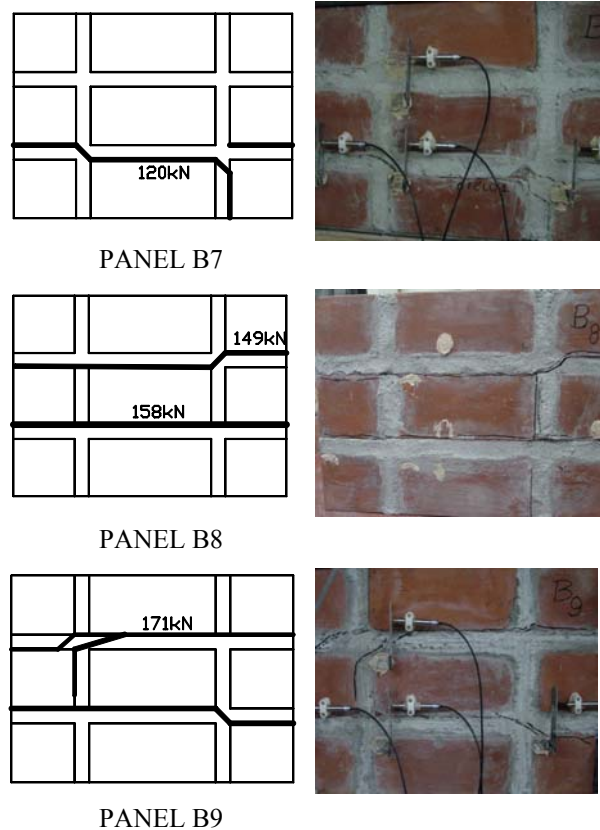


Figure 3-15 – Failure mode of the panels - series 3.

3.3.4 Definition of the Joint Strength Parameters

Table 3-1 gives the values of the shear strength of the panels, which results in an higher shear strength under increasing pre-compression level. The shear strength increased 21.9% for the panels of the series 2, in comparison with the panels of the series 1, and 22.5% for the panels of the series 3, in comparison with the panels of the series 2.

Coulomb friction law, for moderate pre-compression levels, can describe the joint strength behavior. The Coulomb's law provides a linear relationship between the shear stress τ and the normal compression stress σ , given by

$$\tau = c + \tan\phi \sigma \quad (1)$$

Here, c is the cohesion and ϕ is the friction angle of the joint.

Table 3-1 – Shear strength of the panels.

<i>Series</i>	<i>Panel</i>	<i>Shear strength</i> (N/mm^2)	<i>Average shear strength</i> (N/mm^2)
Series 1	B1	1.60	1.60
	B2	1.65	
	B3	1.55	
Series 2	B4	2.06	1.95
	B5	2.17	
	B6	1.63	
Series 3	B7	1.92	2.39
	B8	2.53	
	B9	2.72	

Figure 3-16 shows the relation between the normal stress and the shear strength for all tests, as well as a linear regression carried out with the shear strength average for each series of tests. The correlation coefficient r^2 of the linear regression is 0.997, which indicates an excellent correlation.

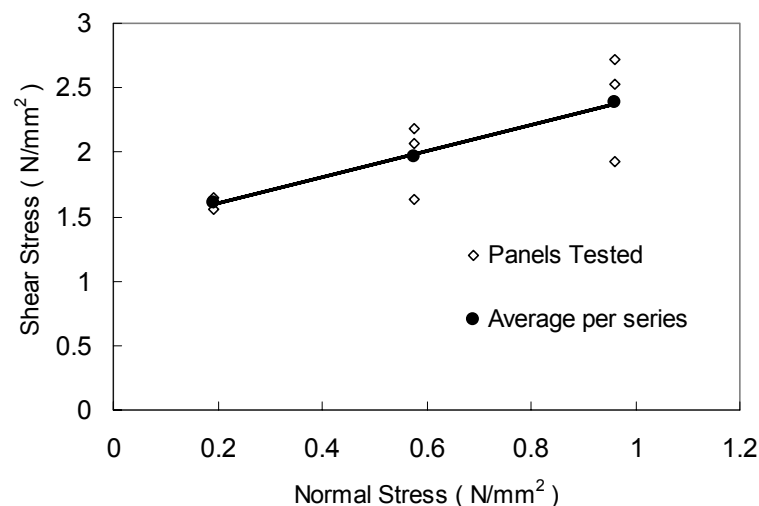


Figure 3-16 – Relation between shear strength and normal stress.

The linear regression indicates a cohesion value c equal to $1.39 N/mm^2$ and a tangent of the friction $\tan\phi$ equal to 1.03. In standard masonry, the value of the

tangent of friction angle seems to range between 0.7 and 1.2, according to different combinations of units and mortars, see van der Pluijm (1999). The value obtained can therefore be considered acceptable. It is also stressed that according to the European Norm EN1052-4 (2000), the characteristic value of the initial shear strength or cohesion is only 80% of the experimental value, or 1.11 N/mm^2 in this case.

3.3.5 Evaluation of the dilatancy

The relation between the normal and the shear displacement is termed dilatancy. This quantity measures the uplift of one unit over the other upon shearing. It is known that the dilatancy decreases under increasing pre-compression levels, see Lourenço (1996). Additionally, dilatancy decreases to zero under increasing shearing displacement due to the smoothing of the sheared surfaces.

Figure 3-17 illustrates the measured dilatancy for panel B3, which is the first panel with recorded significant horizontal displacements. The figure seems to demonstrate that a zero dilatancy is also retrieved for the micro-concrete joints adopted in this case. The complete results for all tests are given in Annex A.

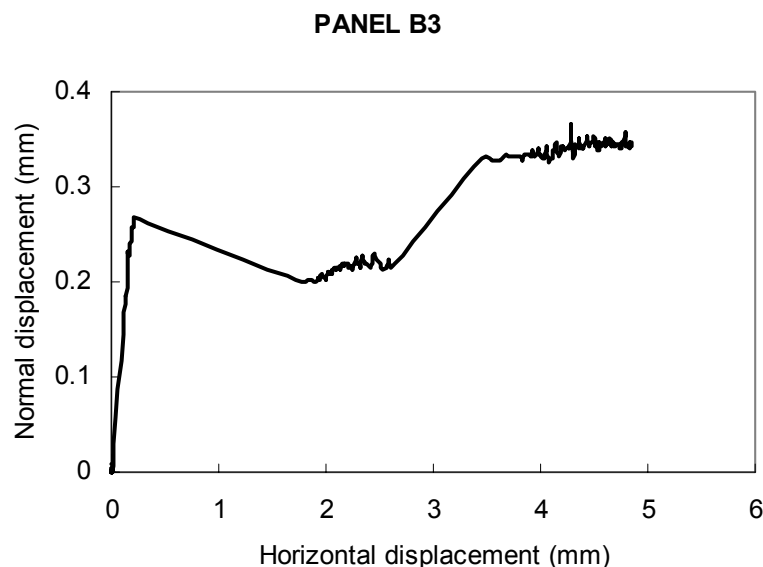


Figure 3-17 – Relation between horizontal and normal displacement, for panel B3.



It is further noted that the given displacements were calculated using the average of displacements recorded by LVDTs 1, 3 and 4 (horizontal displacement) and LVDTs 5, 6 and 7 (normal displacement). The selected horizontal LVDTs (1, 3 and 4) were located on the opposite side of the panel associated with vertical LVDTs (5, 6 and 7). In such a way, the horizontal and vertical displacements were measured in the same location.



4 Conclusions

The masonry units produced by J. Monteiro & Filhos, Lda, for the Isobrick project have been tested under uniaxial compression, resulting in a horizontal strength of 71.8 N/mm^2 and a vertical strength of 32.8 N/mm^2 , based on the apparent cross section. This large anisotropy is due to the extrusion process (moderate influence) and the horizontal holes (major influence).

The micro-concrete adopted for the masonry joints yields a compressive strength of 30.2 N/mm^2 and a tensile flexural strength of 1.73 N/mm^2 .

The triplet test was used successfully to assess the shear behavior of stack bonded masonry with micro-concrete joints. Standard masonry bond is the running bond, which results in discontinuous vertical joints. It is important to stress that the masonry panels studied in this report had continuous vertical joints, just because they will be used to build reinforced masonry shells. Typical failure modes have been obtained and the shear strength seems to adequately follow Coulomb friction law. Therefore, both the use of a stacked configuration and the use of micro-concrete for the joints are acceptable.

The mechanical strength parameters that characterize the interface of the joints is a cohesion c of 1.39 N/mm^2 and a tangent of the friction angle $\tan\phi$ of 1.03. According to EN1052-4 (2000), the characteristic value of the cohesion c is 1.11 N/mm^2 .

It was also found that the dilatancy of the masonry micro-concrete joints, in the stack bond configuration, is similar to standard masonry. In particular, dilatancy tends to zero upon progressive shearing.



5 References

P. Jukes and J. R. Riddington. The Failure of Brick Triplet Test Specimens, *Masonry International*. Vol 15, n^o 1, 2001.

EN 772-1, European Norm for Methods of Test for Masonry Units – Part 1: Determination of compressive strength. June, 2000.

prEN 1052-3 – European Norm for Methods of Test for Masonry – Part 3: Determination of initial shear strength. May, 1996.

EN 1052-4, European Norm for Methods of Test for Masonry – Part 4: Determination of shear strength including damp proof course. May, 2000.

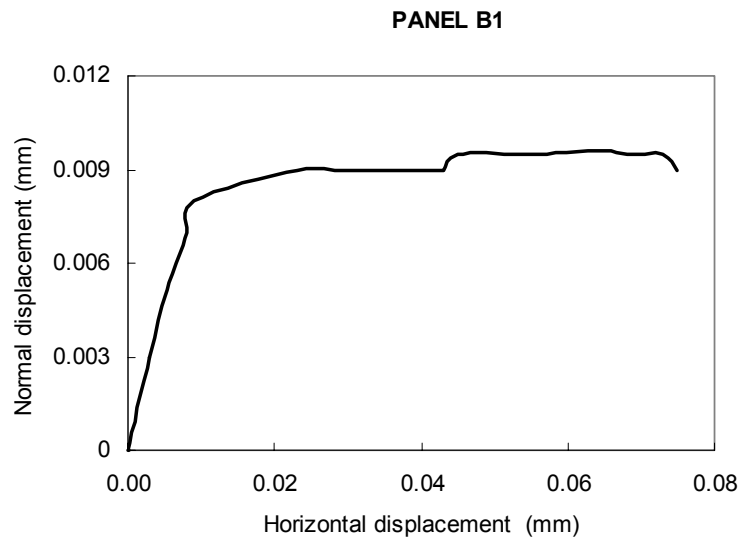
R. v.d. Pluijm. Out of Plane Bending of Masonry Behaviour and Strength. Eindhoven University of Technology. October, 1999.

P.B. Lourenço. Computational Strategies for Masonry Structures. Delft University of Technology. February, 1996.

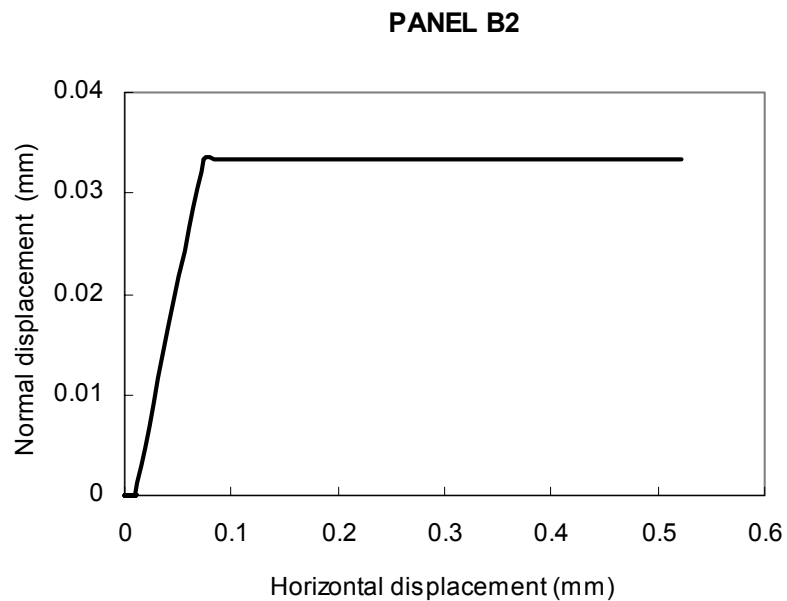
RILEM. Technical Recommendations for the Testing and use of Construction Materials. International Union of Testing and Research Laboratories for Materials and Structures, 1994.



ANNEX A

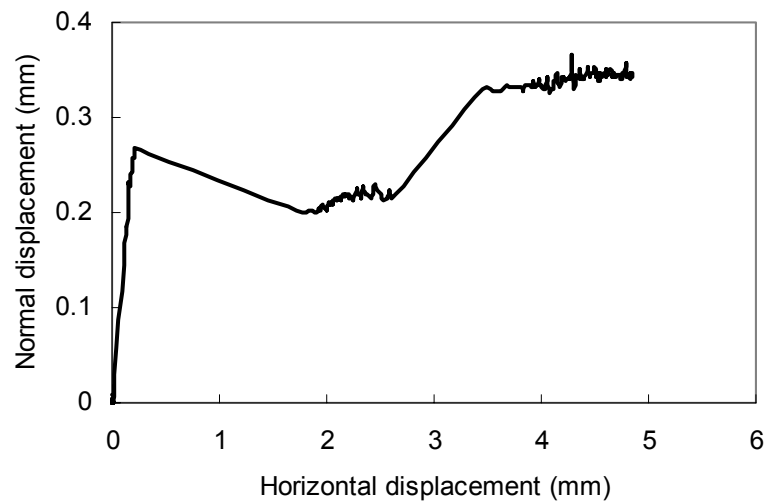


Graphic of average of displacements in shear direction \times displacements in normal direction of panel B1.



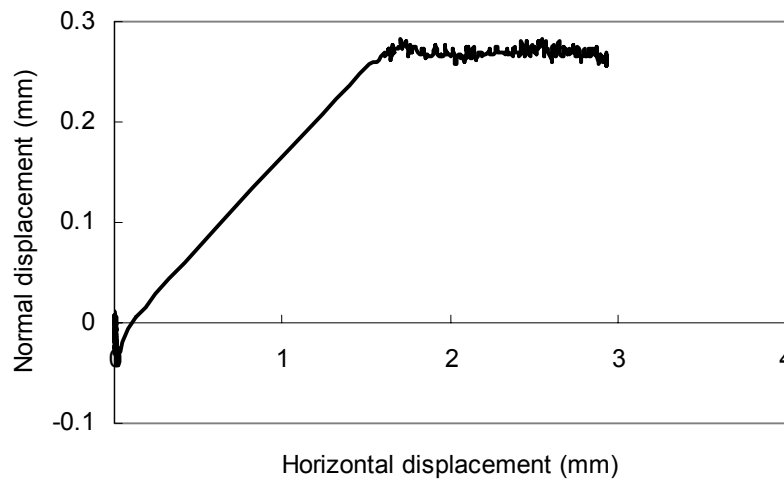
Graphic of average of displacements in shear direction \times displacements in normal direction of panel B2.

PANEL B3



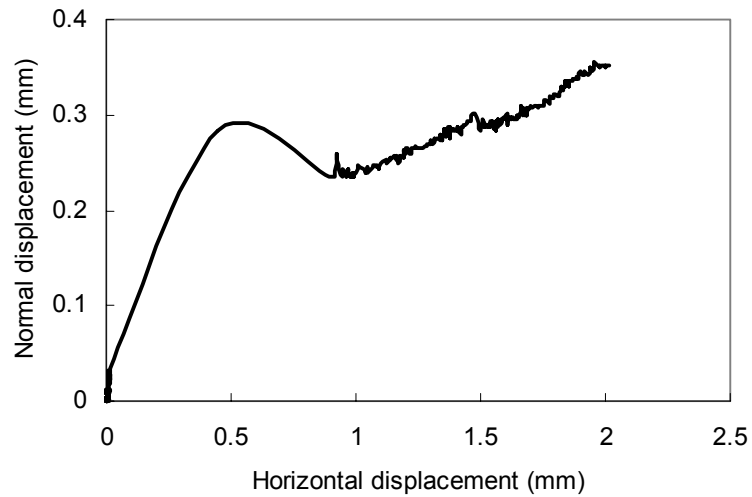
Graphic of average of displacements in shear direction \times displacements in normal direction of panel B3.

PANEL B4



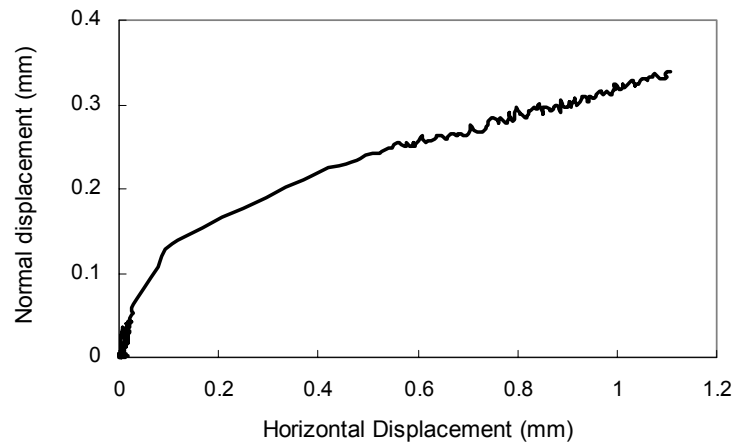
Graphic of average of displacements in shear direction \times displacements in normal direction of panel B4.

PANEL B5



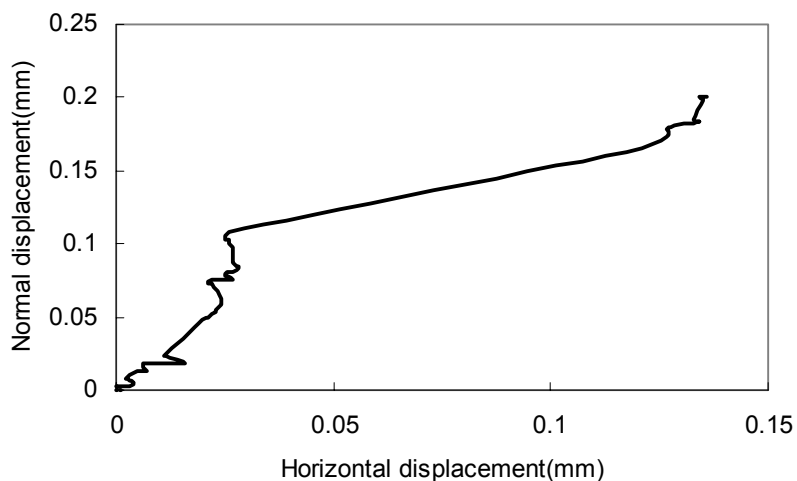
Graphic of average of displacements in shear direction \times displacements in normal direction of panel B5.

PANEL B6



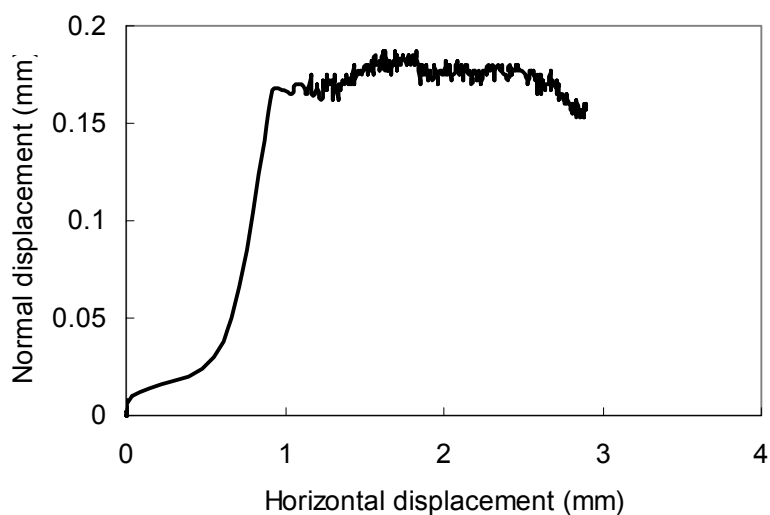
Graphic of average of displacements in shear direction \times displacements in normal direction of panel B6.

PANEL B7

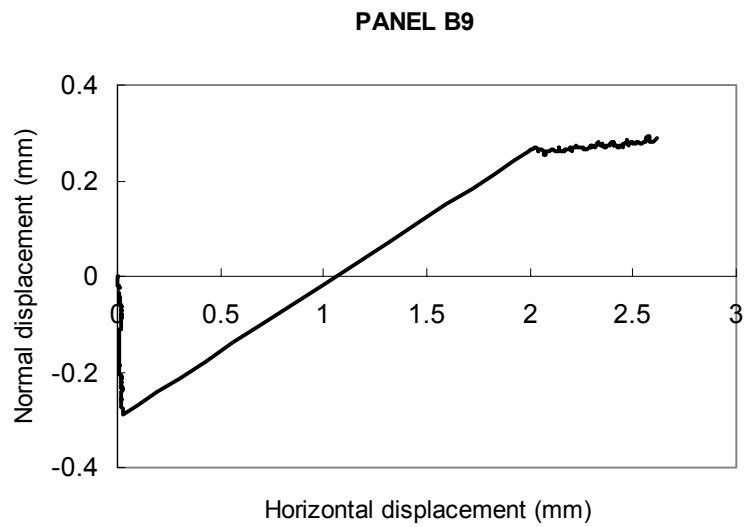


Graphic of average of displacements in shear direction \times displacements in normal direction of panel B7.

PANEL B8



Graphic of average of displacements in shear direction \times displacements in normal direction of panel B8.



Graphic of average of displacements in shear direction \times displacements in normal direction of panel B9.